Published in final edited form as:
Pharm Res. 2011 June ; 28(6): 1317–1327. doi:10.1007/s11095-011-0436-3.

String-Like Micellar Nanoparticles Formed by Complexation of PEG-*b*-PPA and Plasmid DNA and Their Transfection Efficiency

Xuan Jiang,
Department of Materials Science and Engineering, and Whitaker Biomedical Engineering Institute, Johns Hopkins University, 205 Maryland Hall, 3400 North Charles Street, Baltimore, Maryland 21218, USA

Derek Leong,
Department of Materials Science and Engineering, and Whitaker Biomedical Engineering Institute, Johns Hopkins University, 205 Maryland Hall, 3400 North Charles Street, Baltimore, Maryland 21218, USA

Yong Ren,
Department of Materials Science and Engineering, and Whitaker Biomedical Engineering Institute, Johns Hopkins University, 205 Maryland Hall, 3400 North Charles Street, Baltimore, Maryland 21218, USA

Zhiping Li,
Department of Medicine, Johns Hopkins University School of Medicine, 720 Rutland Avenue, Baltimore, Maryland 21231, USA

Michael S. Torbenson, and
Department of Pathology, Johns Hopkins University School of Medicine, 720 Rutland Avenue, Baltimore, Maryland 21231, USA

Hai-Quan Mao
Department of Materials Science and Engineering, and Whitaker Biomedical Engineering Institute, Johns Hopkins University, 205 Maryland Hall, 3400 North Charles Street, Baltimore, Maryland 21218, USA

Hai-Quan Mao: hmao@jhu.edu

Abstract

Purpose—To investigate the gene delivery efficiency of string-like PEG-*b*-PPA/DNA micellar nanoparticles in the liver after intravenous injection and intrabiliary infusion.

Methods—PEG-*b*-PPA/DNA micellar nanoparticles were prepared in aqueous solution through spontaneous self-assembly between plasmid DNA and PEG_{10K}-*b*-PPA_{4K} or PEG_{10K}-*b*-PP_{13K} polymer. The stability of these micellar nanoparticles in different physiological media was evaluated by monitoring the particle size change of micellar nanoparticles with dynamic light scattering (DLS). The transfection efficiency of string-like PEG-*b*-PPA/DNA micellar nanoparticles in the liver was examined and compared with that of PPA/DNA nanoparticles after intravenous and intrabiliary infusion.

Results—These PEG-*b*-PPA/DNA micellar nanoparticles exhibited unique string-like morphology under TEM. The stability of these string-like nanoparticles in salt-, serum- or bile-

Correspondence to: Hai-Quan Mao, hmao@jhu.edu.
Xuan Jiang and Derek Leong contributed equally to this work.

containing media was significantly improved compared with PPA/DNA nanoparticles. More importantly, these PEG-*b*-PPA/DNA nanoparticles mediated 10-fold higher transfection efficiency than PPA/DNA nanoparticles in rat liver when delivered via intrabiliary infusion. In addition, histopathological data revealed that the PEG-*b*-PPA/DNA nanoparticles induced minimal level of liver toxicity or damage.

Conclusions—These string-like PEG-*b*-PPA/DNA micelles can mediate efficient transgene expression in the liver after bile duct infusion, and they have great potential to be used as effective gene carriers for liver-targeted gene delivery.

Keywords

block copolymer; DNA micellar nanoparticles; liver-targeted gene delivery; morphology; string-like

INTRODUCTION

One of the major challenges to nanoparticle-mediated gene delivery *in vivo* is to maintain the stability of nanoparticles in physiological media following administration to blood or different tissues. In these fluids, polyelectrolyte complex particles are subjected to physiological ionic strength buffer, which may destabilize the complexes and release DNA or RNA before they reach the targets. The abundant charged macromolecules can also destabilize the complex or mediate aggregation of the particles. Aggregation of these particles as a result of serum protein adsorption also presents a major challenge. Complement activation is another concern for polymer/DNA complexes with high concentration of hydroxyl (1) or amino groups (2) on particle surface. Recently, self-assembled micellar nanoparticles prepared from plasmid DNA and block copolymers of poly(ethylene glycol) (PEG) and several polycations have been developed as a particularly attractive approach to enhance the colloidal stability of polymer/DNA nanoparticles in physiological media (3–5). The characteristic feature of these micelles is their unique core (polycation/DNA complexes)-shell (PEG) structure. Due to the shielding effect of the PEG corona, these micelles exhibit neutral surface charge at physiological salt concentration that leads to reduced protein adsorption in physiological media. The high hydrophilicity and chain mobility of PEG corona provide additional protection to encapsulated plasmid DNA against enzyme degradation. To date, several successful *in vivo* applications of PEG-*b*-polycation/DNA micelles have been reported, including gene transfer to treat the vascular lesion (6), bone defect in a mouse model (7), and gene delivery to the lung through intratracheal administration (8).

Recently, we have developed a new micellar nanoparticle system based on block copolymers of PEG and polyphosphoramidate (PPA) (9). These PEG-*b*-PPA carriers demonstrated significantly less cytotoxicity than PEI and PPA *in vitro* and *in vivo*. In the first report of this series, we have shown that PEG_{2K}-*b*-PPA_{22K} formed micelles upon complexation with plasmid DNA (5). After bile duct infusion in rats, PEG_{2K}-*b*-PPA_{22K}/DNA micelles mediated significantly enhanced gene expression in liver compared with PPA/DNA nanoparticles because of their better stability in the bile. Since it has been shown that increasing the PEG chain length can significantly enhance the colloidal stability of PEG-coated nanoparticles in physiological medium (10,11), the higher concentration of protein contents in serum and relatively short PEG block length in these micelles may account for the limited improvement in colloidal stability of these micelles.

In the present study, we have synthesized two new PEG-*b*-PPA polymers with higher ratios of PEG block length (10 KDa) to PPA block lengths (4 KDa and 13 KDa, respectively),

characterized the physiochemical properties of these micellar nanoparticles, and assessed the stability of these nanoparticles in salt, serum or bile-containing medium. Their gene delivery efficiency and toxicity in the liver following intravenous and intrabiliary infusion were also characterized in comparison with PPA/DNA nanoparticles.

MATERIALS AND METHODS

Materials

Methoxy PEG (mPEG, Mw=9.5 KDa) was purchased from NOF corporation, Japan. Polyethylenimine (PEI, branched, Mw=25 KDa), carbon tetrachloride (CCl_4), N, N-dimethylformamide (DMF), dichloromethane (DCM), triethylamine (TEA), dipropyltriamine (DPA), triisobutylaluminum (TIBA), ethidium bromide and all other reagents were purchased from Sigma-Aldrich (St. Louis, MO), unless otherwise specified. Fetal bovine serum was purchased from HyClone (Logan, UT). Penicillin-streptomycin and Dulbecco's Modified Eagle's Medium (DMEM) were purchased from Invitrogen (Carlsbad, CA). N^1,N^9-bis(trifluoroacetyl) dipropyltriamine (TFA-DPA) was synthesized according to the procedure reported by O'Sullivan *et al.* (12). The cyclic monomer 4-methyl-2-oxo-2-hydro-1,3,2-dioxaphospholane was prepared as reported previously (13).

Synthesis of PEG-*b*-PPA Copolymers

The synthesis of PEG-*b*-PPAs with DPA side chain, hereafter termed PEG-*b*-PPAs, is summarized in Scheme 1. Different amounts of mPEG (Mw=9.5 KDa, 8.0 or 3.0 g, 0.8 or 0.3 mmol) were first dried by azeotropic distillation in toluene to remove water associated with the PEG chains and then incubated with equal amount of triisobutylaluminum in 20 ml of dichloromethane for 1 h. The polymerization of 4-alkyl-2-oxo-2-hydro-1,3,2-dioxaphospholane was initiated by injecting 5.3 g (43 mmol) of monomer into initiator solution pre-cooled in an ice bath. The mixture was stirred at 0°C for 48 h. The precursor polymer (1) (Scheme 1) was obtained by removing solvent under vacuum at room temperature. The precursor polymer was then dissolved in 40 ml of anhydrous DMF under argon. To this solution was added 37.8 g (86 mmol) of N^1,N^9-bis(trifluoroacetyl)dipropyltriamine (TFA-DPA), followed by addition of 48.0 ml (340 mmol) of anhydrous triethylamine and 33.3 ml (340 mmol) of anhydrous CCl_4. The mixture was stirred at 0°C for 30 min, then at room temperature for 24 h. The reaction mixture was then precipitated into ether and dried under vacuum to yield polymer (2). Polymer (2) was suspended in 25% ammonia solution and stirred at 60°C for 16 h. The solution was concentrated and dialyzed in dialysis tubing (MWCO 3500, Spectrapor, Spectrum Labs, CA) against distilled water for 2 days with frequent water change. Unreacted mPEG was removed by ion-exchange column (Sephadex C25, Sigma) using DI water as an eluent. Sodium hydroxide (0.1 mol/L) was used to elute the PEG-*b*-PPA polymer. The PEG-*b*-PPA was obtained after neutralization, dialysis and lyophilization (yield 30–40%).

The molecular weights of PEG-*b*-PPA and PPA control were determined using an Agilent 1200 Series Isocratic LC System equipped with PL aquagel-OH 30 8-μm column and PL Aquagel-OH MIXED 8-μm column (Polymer Laboratories Ltd.), which was connected with a multi-angle light scattering detector (MiniDawn, Wyatt Technology, Santa Barbara, CA). A dn/dc value of 1.4 was used for all PEG-*b*-PPA samples. Sodium acetate buffer (HAc 0.5 M and NaAc 0.5 M) was used as the mobile phase (flow rate= 0.5 ml/min). The ^{1}H-NMR spectra were recorded on a Bruker 400 MHz NMR (Bruker, Billerica, MA). The grafting degree (p/m, Scheme 1) was obtained by comparing the integral of peaks at δ=1.1–1.4 ppm ($C\underline{H}_3$- on the backbone) and δ=1.9–2.0 ppm ($-CH_2C\underline{H}_2CH_2-$ in the graft).

Amplification and Purification of Plasmid DNA

VR1255C plasmid DNA (6.4 Kb, CMV promoter) encoding firefly luciferase was a gift from Vical (San Diego, CA). The plasmid DNA was amplified in E. coli DH5α and purified with QIAGEN EndoFree Giga kits (QIAGEN, Valencia, CA) according to manufacturer's protocol.

Preparation of PEG-*b*-PPA/DNA Micelles

For a typical preparation of PEG-*b*-PPA/DNA micelles, plasmid DNA solution (250 μL) in DI water at a concentration of 50 μg/ml was added to an equal volume of PEG-*b*-PPA solution in DI water at various concentrations, which corresponded to different N/P ratios. The mixture was vortexed for 20 s and incubated for 30 min at room temperature before characterization or transfection experiments.

Compaction Ability of PEG-*b*-PPA Copolymers

PEG-*b*-PPA/DNA micelle solutions at different N/P ratios were prepared by mixing 25 μL VR1255 DNA solution in DI water at a concentration of 20 μg/ml with an equal volume of PEG-*b*-PPA solution in DI water at various concentrations. The mixture was incubated for 30 min at room temperature, and then subjected to electrophoresis on a 0.8% (w/v) agarose gel for 40 min at 80 V. The gel was stained with ethidium bromide and visualized on a UV illuminator (Eagle Eye II, Stratagene, La Jolla, CA).

Size and Zeta Potential of PEG-*b*-PPA/DNA Micelles

The particle size and zeta potential of PEG-*b*-PPA/DNA micelles were determined by dynamic light scattering (DLS) and laser Doppler anemometry, respectively, using a ZS90 Zetasizer (Malvern Instruments, Southborough, MA). DLS measurement was carried out at 25°C, and the scattering angle was fixed at 90°. The data was analyzed by a cumulative method to obtain the number mean hydrodynamic diameter. The laser Doppler electrophoresis measurements were performed using an aqueous dip cell in the automatic mode, and the zeta potential was calculated using the Smoluchowski equation.

Transmission Electron Microscopy

Ten μL of PEG-*b*-PPA/DNA micelles were added to an ionized 400-mesh nickel Formvar/Carbon film TEM grid (Electron Microscope Sciences, Hatfield, PA) and incubated for 5 min at 25°C, followed by washing with deionized water. The grid was further stained with uranyl acetate (1% solution) for 1 min and air-dried for 10 min before imaging. TEM images were obtained with a FEI Tecnai 12 Twin 120 kV TEM.

In Vitro Gene Transfection

In vitro transfection of PEG-*b*-PPA/DNA micelles was carried out in HEK293 cells. HEK293 cells were maintained in Dulbecco's Modified Eagle's Medium supplemented with 10% fetal bovine serum at 37°C and 5% CO_2. Cells were seeded in 24-well plates at a density of 8×10^4 cells per well one day before transfection. PEG-*b*-PPA/DNA micelles or PPA/DNA nanoparticles containing 2 μg of plasmid DNA were added to each well. The culture media were replaced 4 h after the addition of PEG-*b*-PPA/DNA micelles or PPA/DNA nanoparticles. Two days after transfection, the culture media were removed, and cells were washed with 0.5 ml of phosphate-buffered saline (pH 7.4). Cells in each well were then lysed with 200 μL reporter lysis buffer (Promega, Madison, WI) and subjected to two freeze-thaw cycles. The lysate was centrifuged at 14,000 rpm for 5 min. Twenty μL of cell lysate supernatant was mixed with 100 μL of luciferase substrate (Promega, Madison, WI), and the luciferase activities were measured on a luminometer (20/20n Single Tube luminometer, Turner BioSystems, Sunnyvale, CA). The luciferase activity was converted to

the amount of luciferase using recombinant luciferase (Promega, Madison, WI) as the standard and normalized against protein content using the BCA protein assay (Bio-Rad Laboratories, Hercules, CA).

Gene Delivery in Mice Through Tail Vein Injection

Female Balb/c mice aged 8–10 weeks (20–25 g) were grouped randomly. Cl_2MDP liposomes were prepared as described in the literature (14). Mice were first treated with Cl_2MDP liposomes (20 μL/mouse) through tail vein injection to remove the Kupffer cells in the liver. One day after the treatment, mice were injected with 250 μL of PEI/DNA nanoparticles (*N*/*P*=10), PPA/DNA nanoparticles or PEG-*b*-PPA/DNA micelles (*N*/*P*=8) containing 25 μg VR1255 DNA in 5% glucose solution through tail vein over 30 s. After another 24 h, the mice were sacrificed, and major organs (liver, heart, lung, spleen and kidney) were harvested, weighed and homogenized with a tissue homogenizer (Heidolph, Schwabach, Germany). The homogenate was subjected to two freeze-thaw cycles and centrifuged at 14,000 rpm for 5 min at 4°C. Luciferase activity was analyzed as described above and normalized against the weight of whole tissue. The animal experiments were performed according to the protocol approved by the Animal Care and Use Committee at Johns Hopkins University School of Medicine.

Gene Delivery in Rats Though Intrabiliary Infusion

The animal experiments were performed according to a protocol approved by the Animal Care and Use Committee at Johns Hopkins University School of Medicine. Male Wistar rats aged 6–8 weeks (200–300 g) were grouped randomly. The rats were anesthetized with intraperitoneal (IP) injection of Ketamine (100 mg/kg) and Xylazine (10 mg/kg). A 33-gauge needle was inserted into the common bile duct, and the needle was secured by tying around the common bile duct. Four ml of PEG-*b*-PPA/DNA micelles (*N*/*P*=8) or PPA/DNA nanoparticles (*N*/*P*= 8) containing 20 μg VR1255 DNA in 5% glucose solution were infused through the bile duct over 20 min with a syringe pump. A tie was then placed around the bile duct between the liver and the point of infusion to prevent back flow before the needle was withdrawn. Occasionally, stitches with 10-O nylon (Ethicon, Somerville, NJ) were needed to repair the needle hole in the bile duct to prevent bile leakage. Three days after administration, rats were sacrificed, and major organs (liver, heart, lung, spleen and kidney) were harvested, weighed and homogenized with a tissue homogenizer (Heidolph, Schwabach, Germany). The homogenate was subjected to two freeze-thaw cycles and centrifuged at 14,000 rpm for 5 min at 4°C. Luciferase activity was analyzed as described above and normalized against the weight of whole tissue.

Evaluation of Liver Toxicity

Three days after bile duct infusion, liver tissue from different lobes of the rat liver was isolated for histochemical analysis. The tissue was washed with phosphate-buffered saline (pH 7.4) and then fixed in phosphate-buffered formalin (4%) overnight. Tissue sectioning and H&E staining of sectioned tissues were performed by the Pathology Lab at Department of Comparative Medicine, Johns Hopkins School of Medicine. The histopathological examination was conducted in a blinded fashion.

RESULTS

Synthesis of PEG_{10K}-*b*-PPA Copolymers

To prepare PEG_{10K}-*b*-PPA polymer, $mPEG_{10K}$-OH was first reacted with triisobutylaluminum (TIBA) at 1:1 molar ratio to obtain the macroinitiator (Scheme 1). Although the mechanism for the polymerization of phosphocyclic monomer with TIBA

remains to be fully elucidated, the propagation is most likely mediated by ring opening at the P-O bond of the coordinating monomer (15). By varying the monomer to macroinitiator ratio, two PEG_{10K}-*b*-PPA carriers with PPA block lengths of 4 kDa and 13 KDa (Table I) were obtained. However, the theoretical molecular weights of PPA block for these two polymers were 10 KDa and 28 KDa, respectively. The difference between the actual molecular weight and theoretical molecular weight may be partially explained by the low conversion of the monomer to polymer and the hydrolyzation of PPA backbone during the removal of trifluoroacetate. The grafting degree of DPA in PEG_{10K}-*b*-PPA (Scheme 1), which is defined by the fraction of repeating units grafted with DPA side chain and determines the net positive charge density of PPA block, was obtained by comparing the integral of peaks at δ 1.1–1.4 ppm ($C\underline{H}_3$ in the backbone) with that at δ 1.6–2.0 ppm ($CH_2C\underline{H}_2CH_2$ on the side chain) on the ^{1}H-NMR spectrum (13). As shown in Table I, not all the repeating units on the polyphosphoester backbone were grafted with DPA, and the grafting degrees of DPA for PEG_{10K}-*b*-PPA_{4K} and PEG_{10K}-*b*-PPA_{13K} polymers were 54.3% and 48.9%, respectively. This is probably due to the steric hindrance of TFA-DPA.

Synthesis and Characterization of PEG_{10K}-*b*-PPA/DNA Micelles

The compaction abilities of these two PEG_{10K}-*b*-PPA polymers were evaluated by gel electrophoresis assay. As shown in Fig. 1a, PPA_{4K} and PPA_{25K} polymers exhibited high DNA compaction ability, and they could effectively condense plasmid DNA at N/P ratio of less than 1.5. PEG_{10K}-*b*-PPA_{4K} and PEG_{10K}-*b*-PPA_{13K} reached complete retardation of plasmid DNA at N/P ratio of 1.0 and 1.5, respectively, suggesting that DNA binding ability of PEG_{10K}-*b*-PPA polymers was not significantly affected compared with PPAs. The morphology of self-assembled PEG-*b*-PPA/DNA micellar nanoparticles prepared with these two copolymers was characterized with TEM. Both PEG_{10K}-*b*-PPA_{4K} and PEG_{10K}-*b*-PPA_{13K}/DNA micellar nanoparticles were prepared at an N/P ratio of 8. This N/P ratio was chosen because both nanoparticles mediated highest efficiency in the transfection of HEK293 cells in our pilot experiments. Interestingly, both PEG_{10K}-*b*-PPA_{4K} and PEG_{10K}-*b*-PPA_{13K}/DNA micellar nanoparticles appeared to contain a mixture of string-like micelles with lengths between 200 and 800 nm and diameters in 10 to 20 nm range, and ring-like micelles with outer diameters in the range of 80 to 200 nm. In addition, surface charges of these PEG_{10K}-*b*-PPA micelles were significantly lower than those of PPA/DNA nanoparticles (PPAs with molecular weight of 4, 10 and 25 KDa) at the same N/P ratios (Fig. 1d), presumably due to the shielding effect from PEG corona. Judging from the zeta potential measurements, the PEG_{10K}-*b*-PPA_{4K}/DNA nanoparticles were nearly neutral on the surface, and PEG_{10K}-*b*-PPA_{13K}/DNA nanoparticles carried slightly more net positive charges. It is likely that the number of PEG molecule packed on the surface of the PEG_{10K}-*b*-PPA_{4K}/DNA micelles was higher than of PEG_{10K}-*b*-PPA_{13K}/DNA micelles at the same N/P ratio; hence the former provided better shielding effect with lower zeta potential.

Stability of PEG_{10K}-*b*-PPA/DNA Micelles in the Presence of Salt, Serum and Bile

It has been demonstrated that the polyelectrolyte complexes of cationic polymer and DNA can be weakened in the presence of salts due to charge screening effect (16), and residual charges on the nanoparticle surface tend to cause aggregation of nanoparticles in the presence of serum proteins and bile (17–19). The electrostatically neutral and highly mobile PEG corona of the PEG_{10K}-*b*-PPA/DNA micelles can improve the stability of nanoparticles at physiological salt concentration and in the presence of serum and bile. To validate this hypothesis, we measured the particle size of PPA/DNA nanoparticles and PEG_{10K}-*b*-PPA/DNA micelles after incubation with salt at physiological concentration by using a dynamic lighting scattering detector. Here we showed that both sets of PEG_{10K}-*b*-PPA/DNA micelles did not aggregate and displayed the same apparent particle size as that in DI water (Fig. 2a) after 30 min. Among all PPA/DNA nanoparticles tested, PPA_{25K}/DNA nanoparticles

demonstrated the highest stability in salt solution; the number average particle size increased slightly from 61 nm to 85 nm after 30 min of incubation with 0.15 M NaCl. However, PPA_{4K} and PPA_{10K}/DNA nanoparticles were destabilized by salt and the particle size increased dramatically to 840 nm and 378 nm, respectively.

The serum stability of the two sets of PEG_{10K}-*b*-PPA/DNA micelles was evaluated by incubating the micelles with 10% (v/v) fetal bovine serum (FBS). There was no significant change in the particle size of these PEG_{10K}-*b*-PPA/DNA micelles after incubation with 10% FBS for 30 min (Fig. 2b). In contrast, all three PPA/DNA nanoparticles demonstrated poor colloidal stability in the presence of 10% FBS. After 30 min of incubation, the average particle sizes of PPA_{4K}, PPA_{10K} and PPA_{25K}/DNA nanoparticles increased to 948 nm, 1.11 μm and 2.12 μm, respectively.

Given our interest in evaluating the efficiency of these micelles in delivering genes to the liver through intrabiliary infusion (5,17,19), we also tested the stability of PEG_{10K}-*b*-PPA/DNA micelles in bile by adding 10% (v/v) rat bile to micelle solution (Fig. 2c). PEG_{10K}-*b*-PPA_{4K}/DNA micelles demonstrated the highest stability with no significant change in particle size at 30 min after the addition of bile, whereas the size of PEG_{10K}-*b*-PPA_{13K}/DNA micelles increased slowly to around 300 nm, suggesting that the compactness of the PEG corona may influence micelle stability in bile containing medium. In contrast, PPA_{4K}, PPA_{10K} and PPA_{25K}/DNA nanoparticles exhibited poor stability in bile. After the addition of bile, the relative particle size of PPA_{25K}/DNA nanoparticles increased rapidly to an average of 1.1 μm after only 5 min and reached 2.7 μm after 30 min. Similarly, PPA_{4K} and PPA_{10K}/DNA nanoparticles aggregated rapidly, and the particle size grew to 1.3 μm and 1.6 μm, respectively, after incubation with bile for 30 min.

In Vitro Transfection Efficiency of PEG-*b*-PPA/DNA Micelles

The transfection efficiency of PEG_{10K}-*b*-PPA/DNA micelles at different N/P ratios ranging from 5 to 12 was characterized in HEK293 cells. The transfection efficiency of PEG_{10K}-*b*-PPA_{4K}/DNA micelles peaked at N/P ratio of 8, whereas transgene expression for PEG_{10K}-*b*-PPA_{13K}/DNA micelles was less sensitive to N/P ratio (Fig. 3). The transgene expression mediated by PEG_{10K}-*b*-PPA_{13K}/DNA micelles was more than 20-fold higher than that by PEG_{10K}-*b*-PPA_{4K}/DNA micelles. For PPA/DNA nanoparticles, the transfection efficiency increased with the increase in PPA molecular weight. PPA_{25K}/DNA nanoparticles showed the highest efficiency among those tested, reaching a level comparable to that by PEI_{25K}/DNA nanoparticles (*N*/*P*=10). Interestingly, although PEG_{10K}-*b*-PPA_{13K}/DNA micelles (*N*/*P* =8) showed only slightly reduced transfection efficiency compared with PPA_{10K}/DNA nanoparticles, the PEG_{10K}-*b*-PPA_{4K}/DNA micelles were 26-fold less efficient than the counterpart PPA_{4K}/DNA nanoparticles (*N*/*P* =8). The significantly lower transfection efficiency of PEG_{10K}-*b*-PPA_{4K}/DNA micelles can be correlated to their much lowered surface charge (3.4 mV) as compared with PPA_{4K}/DNA nanoparticles (32 mV), as the cell uptake of polymer/DNA nanoparticles has been shown to be highly dependent on their surface charge (18).

In Vivo Transfection Efficiency of PEG-*b*-PPA/DNA Micelles After Delivery Through the Retrograde Intrabiliary Infusion (RII)

We have tested the efficiency of micelles in gene delivery to the liver by RII. PEG_{10K}-*b*-PPA/DNA micelles, PPA_{4K}, PPA_{25K}/DNA and PEI_{25K}/DNA nanoparticles were infused through bile duct to the liver of Wistar rats. As shown in Fig. 4a, PPA_{4K}/DNA nanoparticles (*N*/*P* =8) led to slightly higher transgene expression than PPA_{25K}/DNA nanoparticles (*N*/*P* =8) in the rat liver. More importantly, both sets of PEG_{10K}-*b*-PPA/DNA micelles (*N*/*P* =8) mediated 6- to 10-fold higher transgene expression than PPA_{4K}/DNA nanoparticles, and the

transgene expression levels were similar to that mediated by PEI/DNA nanoparticles (N/P=10). Despite the difference in transfection efficiency, these three gene carriers mediated relatively uniform luciferase expression in different lobes of the liver (Fig. 4b), and no expression was detected in other major organs such as lung, kidney, heart, and spleen (data not shown). This is consistent with our previous findings on the effectiveness of liver-targeted delivery by RII (5,17). Following RII, histopathological examination of liver tissue was conducted to assess the potential damage and toxicity of various particles to liver tissue. Upon histopathological examination of the liver tissue harvested on day 3 after RII, PPA_{25K}/DNA nanoparticles and PEG_{10K}-*b*-PPA/DNA micelles did not induce any noticeable damage to liver tissue (Fig. 5a and b). In contrast, PEI/DNA nanoparticles mediated mild ductular proliferation of the bile ducts (Fig. 5c), portal chronic inflammation and lobular chronic inflammation (Fig. 5d).

DISCUSSION

Several DNA-containing micellar nanoparticle systems based on PEG-*b*-polycation block copolymer carriers have been reported recently. We have also synthesized PEG-*b*-PPA block copolymers and prepared micellar nanoparticles with these block copolymers. Only spherical morphology was reported for PEG-*b*-polycation/DNA micelles, and in the case of PEG_{2K}-*b*-PPA/DNA micelles, both spherical and rod-like morphologies have been observed. In this study, we have shown that string-like and ring-like morphologies can be obtained by self-assembly of DNA with PEG_{10K}-*b*-PPA_{4K} or PEG_{10K}-*b*-PPA_{13K}. These results suggest that the morphology of polycation/DNA nanoparticles can be varied by the structure of PEG-*b*-PPA carrier. More detailed analysis on how structural parameters influence PEG-*b*-PPA/DNA micelle morphology is currently underway.

One of the design criteria for DNA-compacting micellar nanoparticles is to achieve higher colloidal stability and complex stability in physiological media for *in vivo* gene delivery applications. Although both PEG_{10K}-*b*-PPA/DNA micelles demonstrated significantly improved colloidal stability compared to PPA/DNA nanoparticles, we still observed a difference in the bile stability of two PEG_{10K}-*b*-PPA/DNA micelles, which may be attributed to the difference in the surface density of PEG molecules on PEG_{10K}-*b*-PPA/DNA micelles. This hypothesis was supported by the fact that PEG_{10K}-*b*-PPA_{4K}/DNA micelles demonstrated much lower surface charge compared to PEG_{10K}-*b*-PPA_{13K}/DNA micelles at all N/P ratios from 5 to 16. In addition, as shown in Table I, the average molecular weight per charge for PEG_{10K}-*b*-PPA_{4K} polymer is significantly smaller than that of PEG_{10K}-*b*-PPA_{13K} polymer. Therefore, when PEG_{10K}-*b*-PPA_{4K}/DNA micelles and PEG_{10K}-*b*-PPA_{13K}/DNA micelles are prepared at the same N/P ratio, a significantly greater amount of PEG_{10K}-*b*-PPA_{4K} molecules participate in micelle formation. As a result, PEG_{10K}-*b*-PPA_{4K}/DNA micelles likely have a higher number of PEG_{10K} molecules on their surface than PEG_{10K}-*b*-PPA_{4K}/DNA micelles formed at the same N/P ratio. Although higher density of PEG molecules on micelle surface may be beneficial to the enhancement of the stability of PEG_{10K}-*b*-PPA/DNA micelles, it can also contribute to the reduction in transfection efficiency because we have observed the much lower transfection efficiency mediated by PEG_{10K}-*b*-PPA_{4K}/DNA micelles compared with PEG_{10K}-*b*-PPA_{13K}/DNA micelles in the transfection of HEK293 cells.

We used liver-targeted gene delivery as a model to assess the transfection efficiency of these string-like micelles *in vivo*. For liver-targeted gene delivery, the access of DNA or vectors to liver parenchymal cells (hepatocytes) remains a critical barrier. The improved colloidal and complex stability of these micelles will likely reduce the aggregation and sequestration of DNA-containing nanoparticles and improve the access of these nanoparticles to liver parenchymal cells through sinusoidal fenestrae. Even though these string-like micelles

demonstrated significantly improved colloidal stability in serum stability test, they failed to lead to any significant level of transfection efficiency in the liver (data not shown). The highest transgene expression was observed in the lung, though the transgene expression level was also low. It is noteworthy that both PEG_{10K}-*b*-PPA/DNA micelles are composed of string-like micelles with lengths over 200 nm and ring-like particles with diameters over 100 nm. Considering the fact that the average size of fenestrae for mice is about 100 nm (20), the passage of these micelles through fenestrate may be seriously hampered by the geometry and the size of PEG_{10K}-*b*-PPA/DNA micelles, thus resulting in low transfection efficiency in the liver, which may help to explain the inconsistency between the poor *in vivo* transfection efficiency and high colloidal stability of PEG_{10K}-*b*-PPA/DNA micelles following intravenous injection of these micelles. The low cell uptake and cell transfection efficiency may also be a major contributing factor.

To overcome the transport barrier over sinusoidal fenestrae, we also attempted to deliver PEG_{10K}-*b*-PPA/DNA micelles and PPA/DNA nanoparticles through bile duct infusion. Bile duct infusion was achieved by injecting nanoparticles into the biliary tree under mild pressure (17,21–23). We and others have shown that this administration route leads to direct delivery of nanoparticles to hepatocytes, although leakage of nanoparticles to vascular compartment *via* sinusoidal drainage was also observed. The advantage of this delivery route is the direct access to hepatocytes, bypassing KCs lining endothelium. However, the destabilizing effect of bile may still pose serious challenges to successful gene delivery efficiency through bile duct infusion. The major components of bile are proteins (2–20 g/l), bile acids (3–45 g/l), cholesterol (1–3.2 g/l), phospholipids (1.4–8.1 g/l) and other ions (24). Some of these components may interact with polymer/DNA nanoparticles and result in dissociation or aggregation of polymer/DNA nanoparticles. We have shown that PPA/DNA nanoparticles form aggregation in the bile and that their access to hepatocytes through bile canaliculi with size from 0.5–1 μm may be limited. In contrast, both PEG_{10K}-*b*-PPA_{13K}/DNA and PEG_{10K}-*b*-PPA_{4K}/DNA micelles demonstrated significantly smaller particle size and good stability after incubation with 10% bile. This correlated well with the 10-fold higher transgene expression levels mediated by both PEG_{10K}-*b*-PPA/DNA micellar nanoparticles compared with PPA/DNA nanoparticles. The good correlation between the stability of different carriers in bile and their transfection efficiency in the liver suggests that the good colloidal stability of gene carriers in the bile is crucial to the gene delivery to the liver through bile duct infusion.

It is interesting to note the discrepancy in the differential gene expression levels for the two micellar nanoparticle carriers between *in vitro* and *in vivo* transfections. The *in vitro* transfection efficiency of PEG_{10K}-*b*-PPA_{13K}/DNA micelles in the presence of 10% FCS was 42-fold higher than that of PEG_{10K}-*b*-PPA_{4K}/DNA micelles, whereas the transgene expression levels for these two sets of micelles in rat liver following intrabiliary infusion were similar ($p > 0.35$). Since the serum and salt stabilities of these two sets of micelles were similar, the higher *in vitro* transfection efficiency obtained with PEG_{10K}-*b*-PPA_{13K}/DNA micelles may be attributed to their significantly higher surface charges or zeta potential (average ξ potential = +22.2 mV at N/P=8) compared with that of PEG_{10K}-b-PPA_{4K}/DNA micelles (+3.5 mV), as high surface charge has been positively correlated to higher cell surface adsorption and cell uptake. However, higher positive surface charge may result in higher degrees of particle surface adsorption of negatively charged serum proteins and bile components, which can also lead to particle aggregation. We have shown that in 10% bile the average equivalent particle size of PEG_{10K}-*b*-PPA_{13K}/DNA micelles increased from 61 nm to 300 nm after 30 min, in contrast to that of PEG_{10K}-*b*-PPA_{4K}/DNA micelles, which remained unchanged. Even though this particle size range was not likely to limit their access to hepatocytes through bile canaliculi, which was verified by the relative uniform distribution of transgene expression among different lobes of the liver (Fig. 4b), the

increased size of the particles may reduce the cellular uptake efficiency. It is also worth noting that the analysis of particle stability was conducted in 10% bile and 10% serum, respectively, since there is no method available for easy assessment of the colloidal stability of nanoparticles in high concentrations of serum or bile. It is highly likely that full serum and bile may mediate more severe aggregation than we reported here in 10% bile and serum. Nevertheless, our data clearly demonstrated that PEG_{10K}-*b*-PPA_{4K}/DNA micelles exhibited higher colloidal stability than all PEG_{10K}-*b*-PPA_{13K}/DNA micelles, likely as a result of higher PEG surface density on micelle surface as described above.

On the other hand, the high surface PEG packing density on PEG_{10K}-*b*-PPA_{4K}/DNA micelles will likely lead to reduced cell binding and uptake as compared with PEG_{10K}-*b*-PPA_{13K}/DNA micelles. Therefore, the collective outcome is that these micelles may have similar transfection efficiency in the liver. Based on this analysis, PEG_{10K}-*b*-PPA_{4K}/DNA micelles with superior serum stability and bile stability among all other particles tested represent a promising candidate for *in vivo* gene delivery. Conjugating cell-specific ligands to the surface of these micelles will most likely further enhance their gene delivery efficiency.

Although they appeared to be heterogeneous in particle size/shape distribution for PEG_{10K}-*b*-PPA_{4K}/DNA micelle preparations, showing a mixture of “string”-like and “ring”-like morphologies, the preparation has been highly reproducible. The transfection results from the micelles prepared in multiple batches have been highly consistent.

CONCLUSIONS

In this report, we have shown for the first time that string-like micelles can be prepared through self assembly of plasmid DNA and PEG-*b*-PPA block copolymer with a 10-KDa PEG block and a 4-KDa or 13-KDa PPA block. These string-like micelles showed significantly improved colloidal and complex stability in the presence of physiological ionic strength buffer, serum and bile. However, the improved stability may have contributed to the lowered *in vitro* cell transfection efficiency and low liver-targeted transgene expression following intravenous infusion. In contrast, these string-like micelles administered through bile duct infusion achieved 10-fold higher transgene expression in the liver than that of PPA/DNA nanoparticles. More importantly, PEG_{10K}-*b* -PPA/DNA micelles did not mediate any detectable level of toxicity or damage to the liver. These findings suggested that PEG_{10K}-*b*-PPA/DNA micellar nanoparticles are promising for liver-targeted gene delivery.

Acknowledgments

This study was supported by the National Institutes of Health, National Institute of General Medical Sciences under the grant GM073937.

ABBREVIATIONS

PEG	polyethylene glycol
PPA	polyphosphoramidate
RII	retrograde intrabiliary infusion
TIBA	triisobutylaluminum

References

1. Chenoweth DE. Complement activation during hemodialysis-clinical observations, proposed mechanisms, and theoretical implications. Artif Organs. 1984; 8(3):281–7. [PubMed: 6332607]
2. Toda M, Iwata H. Effects of hydrophobicity and electrostatic charge on complement activation by amino groups. ACS Appl Mater Interfaces. 2010; 2(4):1107–13. [PubMed: 20380387]
3. Osada K, Christie RJ, Kataoka K. Polymeric micelles from poly (ethylene glycol)-poly(amino acid) block copolymer for drug and gene delivery. J R Soc Interface. 2009; 6:S325–39. [PubMed: 19364722]
4. Jiang X, Zheng Y, Chen HH, Leong KW, Wang TH, Mao HQ. Dual-sensitive micellar nanoparticles regulate DNA unpacking and enhance gene-delivery efficiency. Adv Mater. 2010; 22(23):2556–60. [PubMed: 20440698]
5. Jiang X, Dai H, Ke CY, Mo X, Torbenson MS, Li ZP, et al. PEG-*b*-PPA/DNA micelles improve transgene expression in rat liver through intrabiliary infusion. J Control Release. 2007; 122(3):297–304. [PubMed: 17640758]
6. Akagi D, Oba M, Koyama H, Nishiyama N, Fukushima S, Miyata T, et al. Biocompatible micellar nanovectors achieve efficient gene transfer to vascular lesions without cytotoxicity and thrombus formation. Gene Ther. 2007; 14(13):1029–38. [PubMed: 17460721]
7. Itaka K, Ohba S, Miyata K, Kawaguchi H, Nakamura K, Takato T, et al. Bone regeneration by regulated *in vivo* gene transfer using biocompatible polyplex nanomicelles. Mol Ther. 2007; 15 (9): 1655–62. [PubMed: 17551504]
8. Harada-Shiba M, Takamisawa I, Miyata K, Ishii T, Nishiyama N, Itaka K, et al. Intratracheal gene transfer of adrenomedullin using polyplex nanomicelles attenuates monocrotaline-induced pulmonary hypertension in rats. Mol Ther. 2009; 17(7):1180–6. [PubMed: 19337232]
9. Mao HQ, Leong KW. Design of Polyphosphoester-DNA Nanoparticles for Non-Viral Gene Delivery. Adv Genet. 2005; 53PA:275–306. [PubMed: 16243068]
10. Mosqueira VC, Legrand P, Morgat JL, Vert M, Mysiakine E, Gref R, et al. Biodistribution of long-circulating PEG-grafted nanocapsules in mice: effects of PEG chain length and density. Pharm Res. 2001; 18(10):1411–9. [PubMed: 11697466]
11. Gref R, Minamitake Y, Peracchia MT, Trubetskoy V, Torchilin V, Langer R. Biodegradable long-circulating polymeric nanospheres. Science. 1994; 263(5153):1600–3. [PubMed: 8128245]
12. Osullivan MC, Dalrymple DM. A one-step procedure for the selective trifluoroacetylation of primary amino-groups of polyamines. Tetrahedron Lett. 1995; 36(20):3451–2.
13. Wang J, Zhang PC, Lu HF, Ma N, Wang S, Mao HQ, et al. New polyphosphoramidate with a spermidine side chain as a gene carrier. J Control Release. 2002; 83(1):157–68. [PubMed: 12220847]
14. Van Rooijen N, Sanders A. Liposome mediated depletion of macrophages: mechanism of action, preparation of liposomes and applications. J Immunol Methods. 1994; 174(1–2):83–93. [PubMed: 8083541]
15. Kuran W. Coordination polymerization of heterocyclic and hetero-unsaturated monomers. Prog Polym Sci. 1998; 23(6):919–92.
16. Voets IK, de Keizer A, Stuart MAC. Complex coacervate core micelles. Adv Colloid Interface Sci. 2009; 147–48:300–18.
17. Dai H, Jiang X, Tan GC, Chen Y, Torbenson M, Leong KW, et al. Chitosan-DNA nanoparticles delivered by intrabiliary infusion enhance liver-targeted gene delivery. Int J Nanomedicine. 2006; 1 (4):507–22. [PubMed: 17369870]
18. Dash PR, Read ML, Fisher KD, Howard KA, Wolfert M, Oupicky D, et al. Decreased binding to proteins and cells of polymeric gene delivery vectors surface modified with a multivalent hydrophilic polymer and retargeting through attachment of transferring. J Biol Chem. 2000; 275(6):3793–802. [PubMed: 10660529]
19. Jiang X, Dai H, Leong KW, Goh SH, Mao HQ, Yang YY. Chitosan-g-PEG/DNA complexes deliver gene to the rat liver via intrabiliary and intraportal infusions. J Gene Med. 2006; 8(4):477–87. [PubMed: 16389625]

20. Steffan AM, Gendrault JL, Kirn A. Increase in the number of fenestrae in mouse endothelial liver cells by altering the cytoskeleton with cytochalasin B. Hepatology. 1987; 7 (6):1230–8. [PubMed: 3679088]

21. Otsuka M, Baru M, Delriviere L, Talpe S, Nur I, Gianello P. *In vivo* liver-directed gene transfer in rats and pigs with large anionic multilamellar liposomes: routes of administration and effects of surgical manipulations on transfection efficiency. J Drug Target. 2000; 8(4):267–79. [PubMed: 11144237]

22. Zhang X, Collins L, Sawyer GJ, Dong X, Qiu Y, Fabre JW. *In vivo* gene delivery via portal vein and bile duct to individual lobes of the rat liver using a polylysine-based nonviral DNA vector in combination with chloroquine. Hum Gene Ther. 2001; 12 (18):2179–90. [PubMed: 11779402]

23. Zhang X, Sawyer GJ, Dong X, Qiu Y, Collins L, Fabre JW. The *in vivo* use of chloroquine to promote non-viral gene delivery to the liver via the portal vein and bile duct. J Gene Med. 2003; 5 (3):209–18. [PubMed: 12666187]

24. Krejci Z, Hanus L, Podstatova H, Reifova E. A contribution to the problems of the pathogenesis and the microbial etiology of cholelithiasis. Acta Univ Palacki Olomuc Fac Med. 1983; 104:279–86. [PubMed: 6222611]

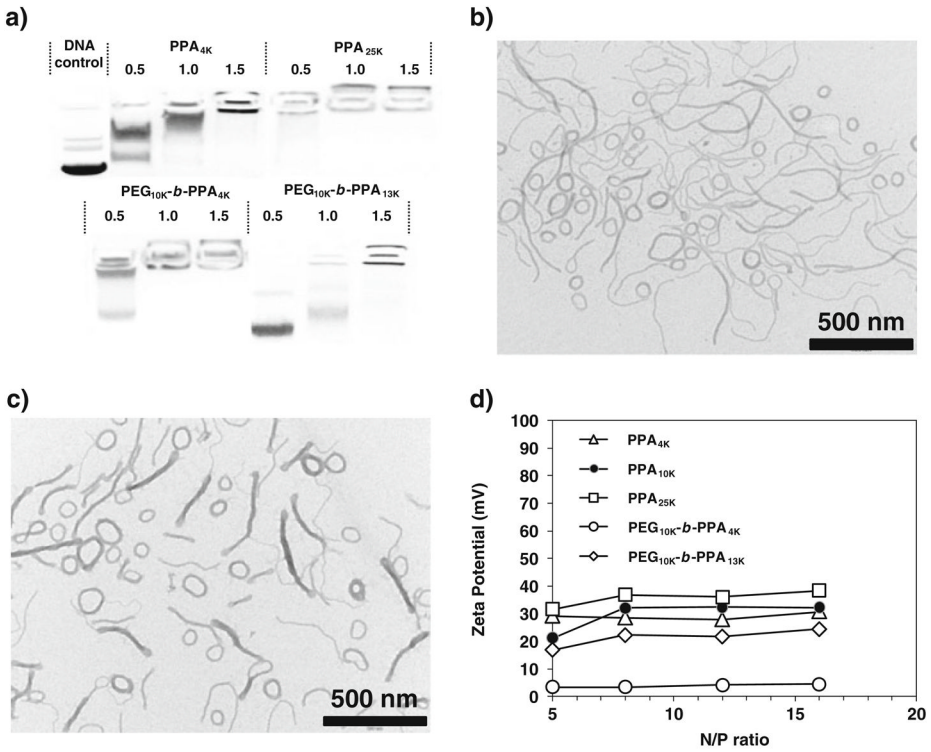

Fig. 1.

a Compaction ability of PPA and PEG_{10K}-*b*-PPA polymers; TEM images of **b** PEG_{10K}-*b*-PPA_{4K}/DNA micelles at N/P=8 and **c** PEG_{10K}-*b*-PPA_{13K}/DNA micelles at N/P=8; **d** Surface charge of PPA/DNA nanoparticles and PEG_{10K}-*b*-PPA/DNA micelles at different N/P ratios.

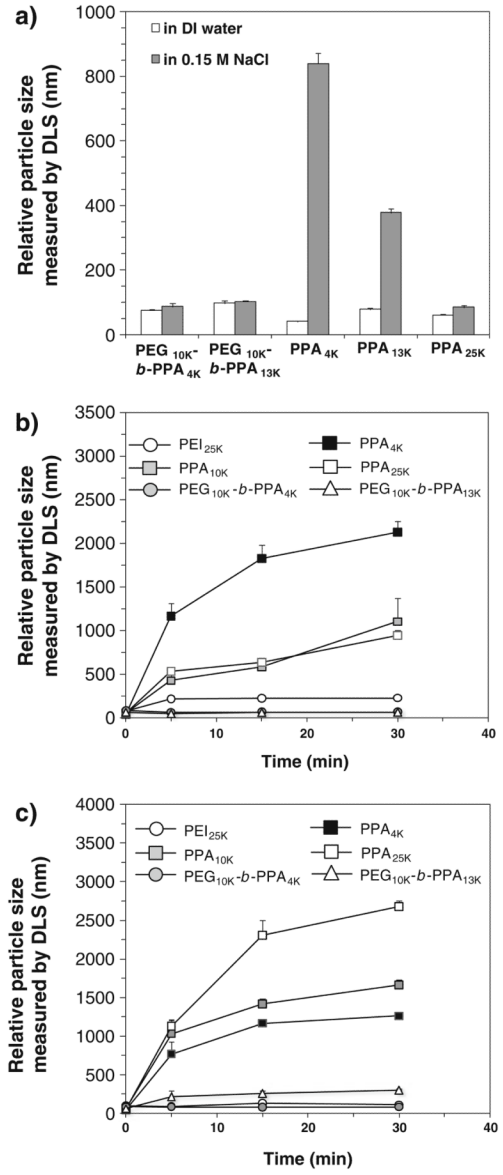

Fig. 2.

Stability of PPA_{4K}, PPA_{10K} and PPA_{25K}/DNA nanoparticles and PEG_{10K}-*b*-PPA/DNA micelles (N/P=8) upon incubation with **a** 0.15 M NaCl, **b** 10% fetal bovine serum and **c** 10% rat bile.

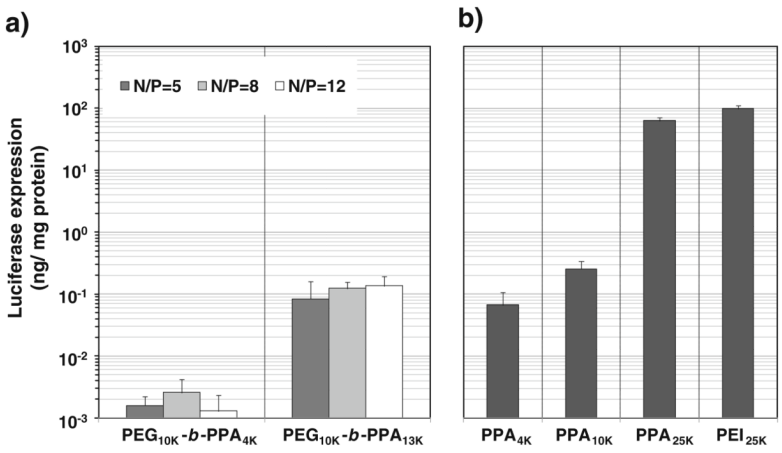

Fig. 3.

Transfection efficiency of **a** PEG_{10K}-*b*-PPA/DNA micelles and **b** PPA/DNA nanoparticles at N/P=8 and PEI/DNA nanoparticles at N/P=10 in HEK293 cells. Each bar represents average± standard division (*n*=4).

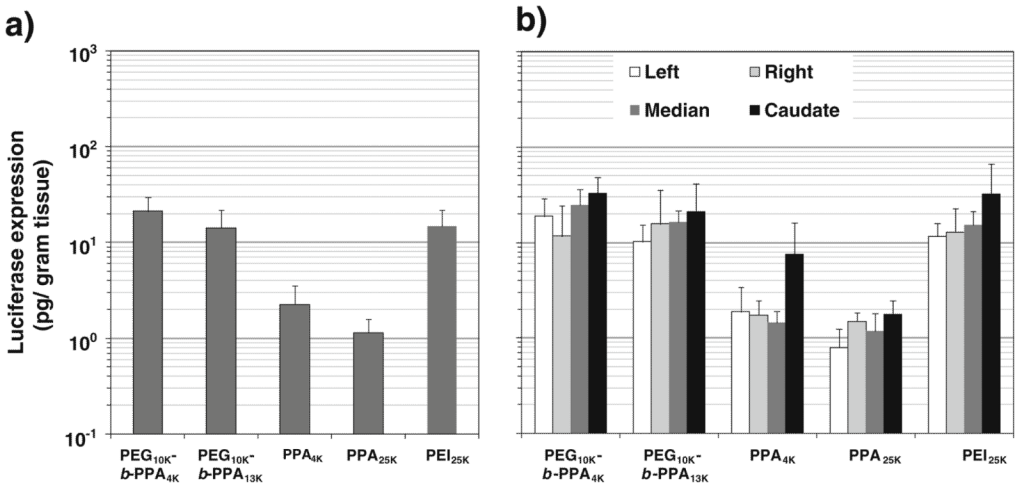

Fig. 4.

Transfection efficiency of PPA/DNA nanoparticles at N/P= 8, PEI_{25K}/DNA nanoparticles at N/P=10 and PEG_{10K}-*b*-PPA/DNA micelles at N/P=8 on day 3 following intrabiliary infusion of Wistar rats at a DNA dose of 20 μg per rat. **a** Overall luciferase expression in the liver. **b** Distribution of luciferase expression in different lobes of the rat liver. Each bar represents average±standard division (*n*=3).

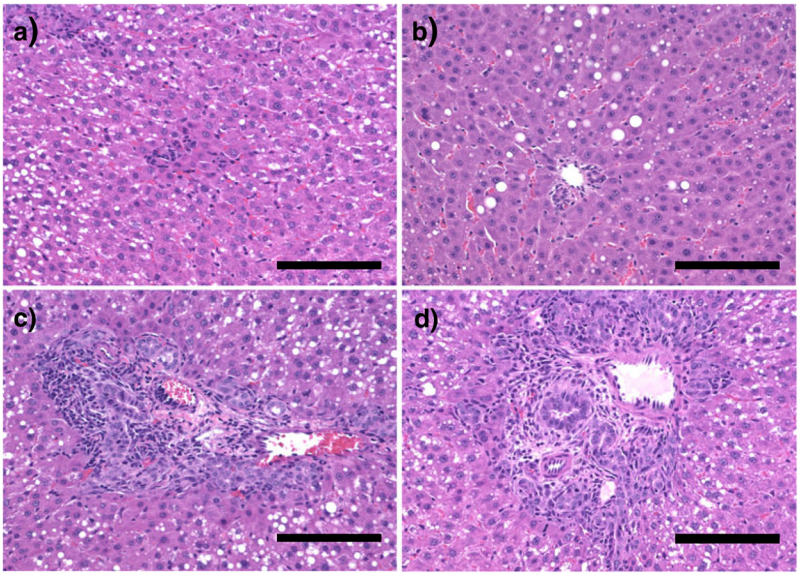

Fig. 5.

H&E stained tissue sections of the portal triad region of liver tissue harvested on day 3 from rats received PEG_{10K}-*b*-PPA_{4K}/DNA micelles at N/P= 8 **a**, PEG_{10K}-*b*-PPA_{4K}/DNA micelles at N/P=8 **b** and PEI_{25K}/DNA nanoparticles at N/P=10 (c, d). The scale bar represents 100 μm.

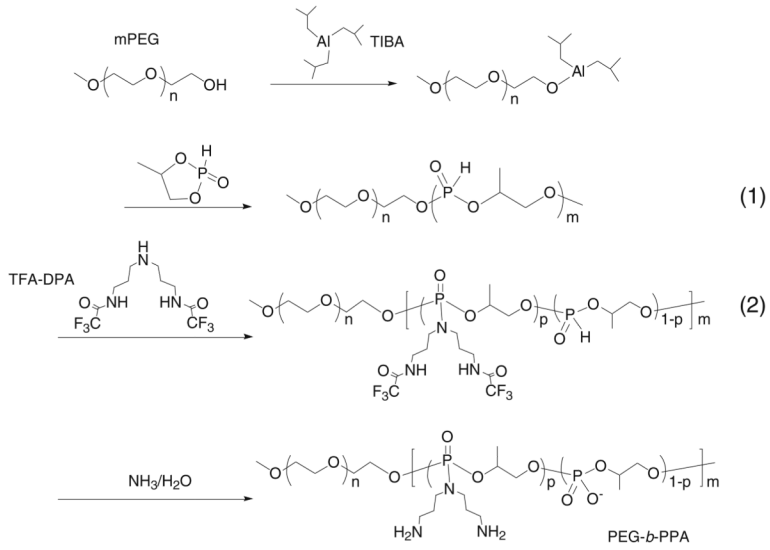

Scheme 1.
Synthesis of PEG_{10K}-*b*-PPA polymers.

Table I

Characterization of Average Molecular Weights and Grafting Degrees of PEG_{10K}-*b*-PPA Polymers

Polymer	**PEG_{10K}-*b*-PPA_{4K}**	**PEG_{10K}-*b*-PPA_{13K}**	**PPA_{4K}**	**PPA_{10K}**	**PPA_{25K}**
Feed ratio of monomer to PEG	53.76	142.86	–	–	–
Target M_n	20,000	38,000	–	–	–
Actual M_n	13,650	22,690	4,400	10.4	25.1
Polydispersity	1.08	1.38	1.64	1.39	2.28
M_n of PPA Block	3,650	12,690			
Average M_n per positive charge	605.3	340.7	–	–	–
Grafting degree of DPA (*p*)[a]	54.3%	48.9%	56.0%	49.6%	57.0%

[a]Percentage of phosphoester units which were grafted with DPA, *p* (see Scheme 1).